Electronic Supplementary Material (ESI) for Nanoscale.

Supplementary Information

High areal capacity lithium sulfur battery cathode by site-selective vapor infiltration of hierarchical carbon nanotube arrays

Rachel Carter[1], Benjamin Davis[2], Landon Oakes[1,2], Matthew R. Maschmann[2], and Cary L. Pint[1, 2, *]

[1] *Department of Mechanical Engineering, Vanderbilt University, Nashville, TN 37235*

[2]*Department of Mechanical & Aerospace Engineering, University of Missouri, Columbia, Missouri 65211, United States*

[2] *Interdisciplinary Materials Science Program, Vanderbilt University, Nashville, TN 37235*

**Corresponding author: cary.l.pint@vanderbilt.edu*

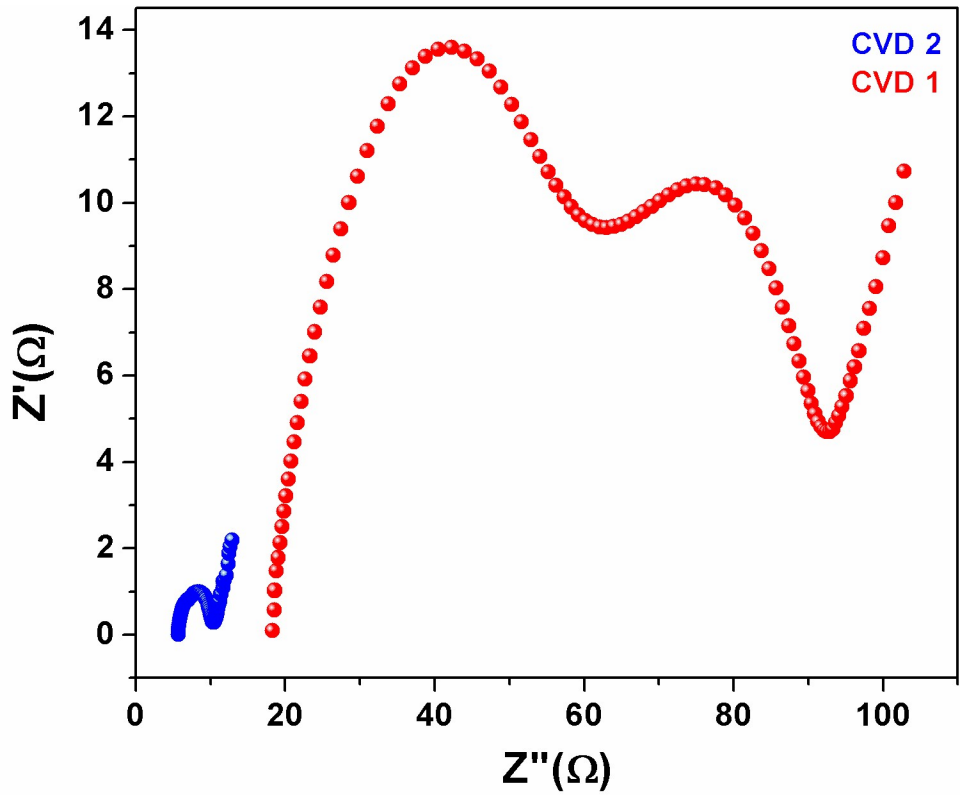

Figure S1- Electrochemical impedance spectroscopy over frequency range (0.05 Hz-1MHz) on both primary and branch cathode on the same axis.

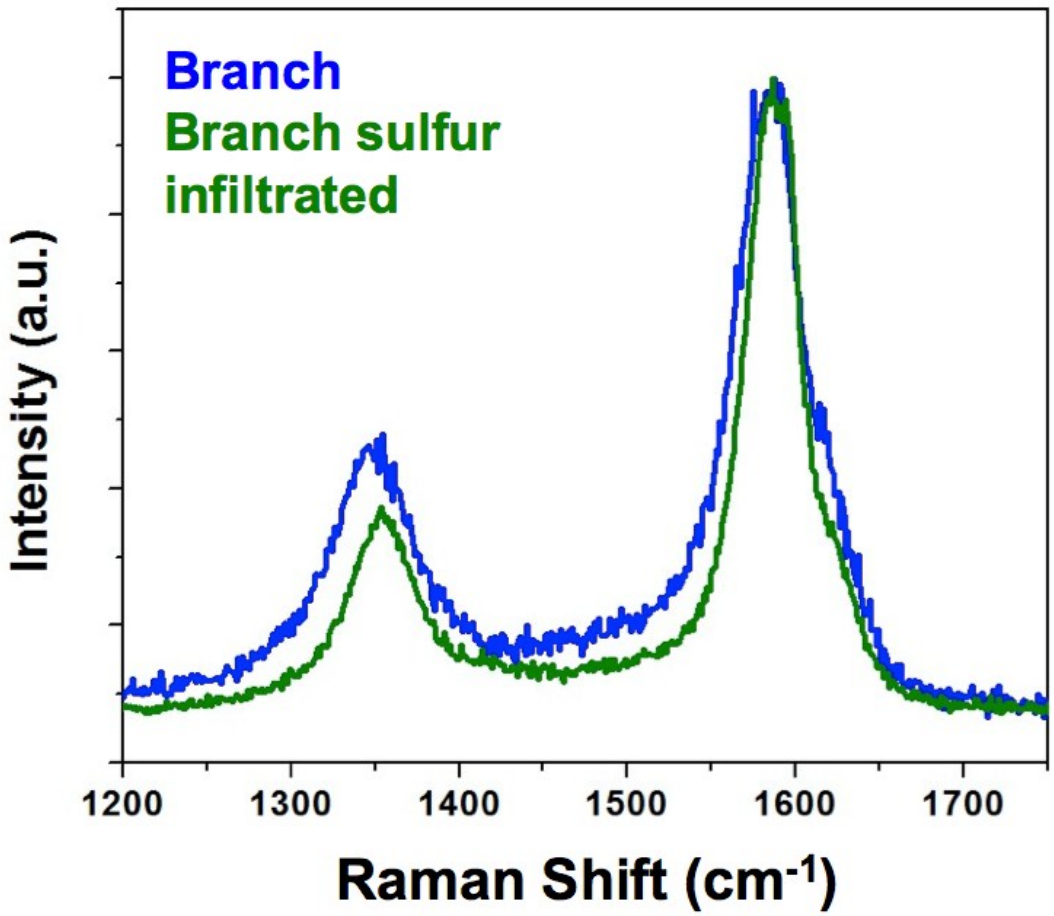

Figure S2- Raman spectroscopy characterization of hierarchical CNTs before and after branch CNTs are isothermal vapor infiltrated with sulfur.

Porosity Calculation

In order to assess the porosity of the sulfur infiltrated material, and determine the capability of the material in accommodating the large volume expansion on discharge, we consider the case where we target filling of the small diameter population of CNTs with sulfur, where our images indicates the filling of CNT interiors with sulfur. Based on an average inner diameter of 4.7 nm of the secondary CNTs derived from ImageJ analysis of over 30 CNTs (representative TEM

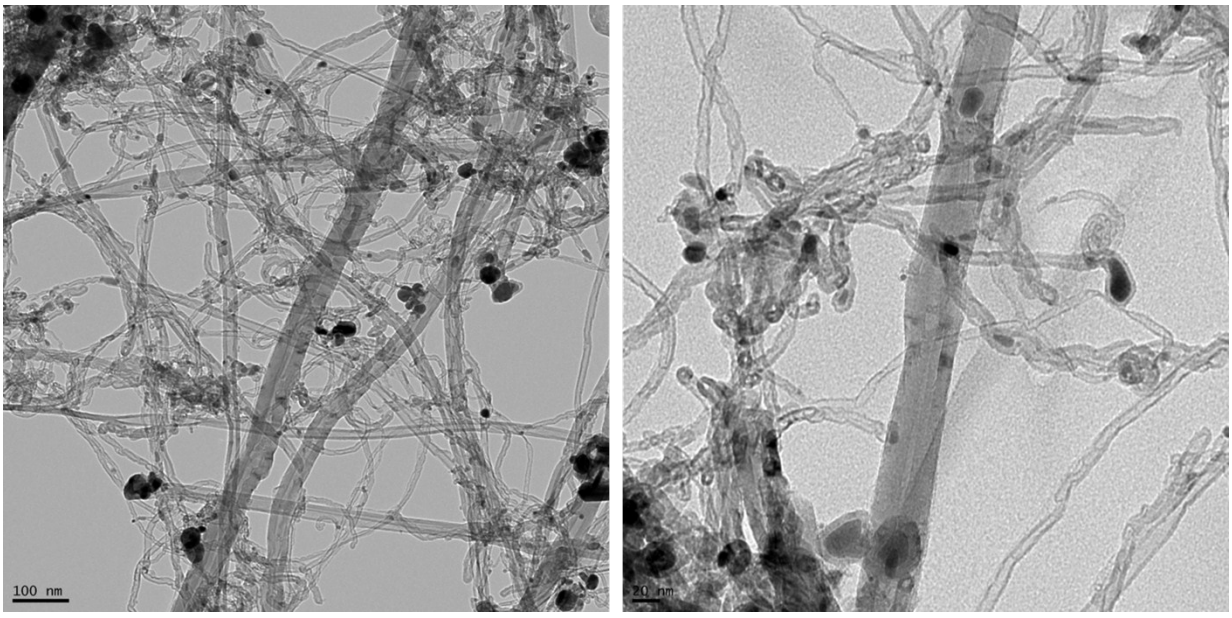

Figure S3- TEM images showing the pore sizes of branch CNTs (small diameter CNTs). Based on TEM analysis, branch CNTs were observed to exhibit average inner diameter of 4.7 nm.

images provided in Figure S3), and information obtained from the growth conditions, we are able to assess the filling fraction of sulfur on the interior versus exterior portion of the branch CNTs.

Portion of Sulfur interior filling (preferential over coating):

$$interior\ loading = \frac{\rho_s \pi r_i^2 L}{\rho_c \pi \left(r_o^2 - r_i^2\right) L + \rho_s \pi r_i^2 L} = 34\%$$

Where ρ_s is density of sulfur, 2.07 g/cm^2, ρ_c is density of CNTs, 2.1 g/cm^2, r_i is CNT average inner CNT radius, which is half the inner diameter, 4.7 nm, as assessed using imageJ from >30 CNTs as seen in the included TEM image, Figure S3, r_O is average outer radius, half the OD reported in Figure 3d, 8 nm. Finally L is CNT length which does not require explicit assessment as it cancels away. Therefore, since a mass loading of 60% is observed, 26% is thus required to

be situated on the CNT exterior. To take this into account on how this coating influences the porosity, we prescribed an effective radius for branched CNTs, or r_s, where this is the radius with the additional 26% of sulfur distributed across the CNT surface.

$$0.26 = \frac{\rho_s\left(r_s^2 - r_o^2\right)}{\rho_s\left(r_s^2 - r_o^2\right) + \rho_c\left(r_o^2 - r_i^2\right)}$$

The resultant radius is 4.4 Angstroms, meaning CNT diameter is only enhanced by 0.8 nm from 8nm to 8.8nm with sulfur loading. Further by calculating the scaffold volume and loading material volumes, the ability of the material to accommodate discharge is verified.

Scaffold volume= (surface area)*(primary growth height)=(1 cm^2)*(0.015 cm)= 0.015 cm^3

Volume of carbon deposited= (mass of deposition)/(density of CNTs)= (0.004 g)/(2 g/cm^3)= 0.002 cm^3

Volume of sulfur deposited= (mass of sulfur)/density of sulfur= (0.006 g)/(2.07 g/cm^3)= 0.0029

Volume of sulfur after expansion (if complete conversion to Li2S is observed)= volume of sulfur deposited*1.8 = 0.0052

With these material volumes, porosity can be assessed.

Porosity of scaffold= 1-(volume of carbon)/(scaffold volume)= 1- (0.002/0.015)= **86.67%**

Porosity after sulfur loading=1-(volume of carbon+ volume of sulfur)/(entire volume)= 1-(0.002+0.0029)/0.015= **67.3%**

Porosity after discharge=1-(volume of carbon+ volume of sulfur)/(entire volume) 1-(0.002+0.0052)/0.015= **52%**

This final discharge porosity assures not only accommodation of the product but also electrolyte accessibility to enable subsequent charge-discharge behavior.

Reference key for Figure 5

A. Y. L. Ding, P. Kopold, K. Hahn, P. A. van Aken, J. Maier, Y. Yu, Adv Funct Mater **2016**, 26, 1112-1119

B. X. X. Gu, C. J. Tong, B. Wen, L. M. Liu, C. Lai, S. Q. Zhang, Electrochim Acta **2016**, 196, 369-376

C. G. J. Hu, C. Xu, Z. H. Sun, S. G. Wang, H. M. Cheng, F. Li, W. C. Ren, Adv Mater **2016**, 28, 1603-1609;

D. F. Y. Jin, S. Xiao, L. J. Lu, Y. Wang, Nano Lett **2016**, 16, 440-447;

E. G. Li, J. H. Sun, W. P. Hou, S. D. Jiang, Y. Huang, J. X. Geng, Nat Commun **2016**, 7, 10601;

F. X. Liang, Y. Rangom, C. Y. Kwok, Q. Pang, L. F. Nazar, Adv. Mater. **2016**, 29, 1603040;

G. P. Lv, J. M. Zheng, Q. Y. Li, X. Xie, S. Ferrara, Z. M. Nie, L. B. Mehdi, N. D. Browning, J. G. Zhang, G. L. Graff, J. Liu, J. Xiao, Adv Energy Mater **2015**, 5, 1402290;

H. L. Ma, H. L. L. Zhuang, S. Y. Wei, K. E. Hendrickson, M. S. Kim, G. Cohn, R. G. Hennig, L. A. Archer, Acs Nano **2016**, 10, 1050-1059;

I F. Wu, Y. Ye, R. Chen, T. Zhao, J. Qian, X. Zhang, L. Li, Q. Huang, B. Xuedong, Y. Cui, Adv. Energy Mater. **2017**, 7, 1601591;

J. X. F. Yang, Y. Yu, N. Yan, H. Z. Zhang, X. F. Li, H. M. Zhang, J Mater Chem A **2016**, 4, 5965-5972;

K. G. M. Zhou, L. Li, C. Q. Ma, S. G. Wang, Y. Shi, N. Koratkar, W. C. Ren, F. Li, H. M. Cheng, Nano Energy **2015**, 11, 356-365.

L Z. Yuan, H.-J. Peng, J.-Q. Huang, X.-Y. Liu, D.-W. Wang, X.-B. Cheng and Q. Zhang, *Adv Funct Mater*, 2014, **24**, 6105-6112.

M R. Ummethala, M. Fritzsche, T. Jaumann, J. Balach, S. Oswald, R. Nowak, N. Sobczak, I. Kaban, M. H. Rümmeli and L. Giebeler, *Energy Storage Materials*, DOI: https://doi.org/10.1016/j.ensm.2017.04.004.

N J. Bruckner, S. Thieme, H. T. Grossmann, S. Dorfler, H. Althues and S. Kaskel, *J Power Sources*, 2014, **268**, 82-87.

O J. Q. Huang, Q. Zhang, S. M. Zhang, X. F. Liu, W. C. Zhu, W. Z. Qian and F. Wei, *Carbon*, 2013, **58**, 99-106.